Structures, Vibrational Frequencies, and Normal Modes of Substituted Azo Dyes: Infrared, Raman, and Density Functional Calculations

Nandita Biswas[†] and Siva Umapathy*

Department of Inorganic and Physical Chemistry, Indian Institute of Science, Bangalore-560012, India

Received: August 19, 1999; In Final Form: November 30, 1999

The vibrational structures of 4-nitro-azobenzene (NAB), 4-(dimethylamino)-azobenzene (DAB), and 4-nitro,4′-(dimethylamino)-azobenzene (NDAB) are of interest due to their importance in optoelectronic applications as well as the unique isomerization mechanism involving the inversion process (at the nitrogen site). In this paper, we present the Fourier transform infrared (FTIR) and Raman spectral studies of NAB, DAB, and NDAB and also report their equilibrium structures, harmonic frequencies, and normal mode assignments, employing the hybrid Hartree−Fock/density functional (HF/DF) method with the 6-31G basis set. The results of the optimized molecular structure obtained on the basis of B3LYP with 6-31G basis set suggest a greater conjugation and π-electron delocalization for the substituted azo dyes in comparison to the parent azo molecule, viz. *trans*-azobenzene (TAB). It is found that the B3LYP/6-31G method is very accurate in predicting harmonic vibrational frequencies and the normal modes for the substituted azo dyes and their isotopic analogues. On the basis of the B3LYP/6-31G force field, the infrared intensities for NAB, DAB, and NDAB, and their isotopomers, are calculated and then compared with those observed experimentally. Finally, the main differences in the vibrational spectra of the substituted azobenzene derivatives are discussed from an analysis of the normal modes.

Introduction

The structure of azo dyes have attracted considerable attention,[1] in recent times, since they represent the largest class of dyes used in industry[2] and also find extensive applicability in analytical chemistry as acid−base, redox and metallochromic indicators. Moreover, azo dyes find wide applicability for reversible optical data storage[3−8] (both holographic and digital). The storage process utilizes the light induced *trans*−*cis*−*trans* isomerization of the azo dye, thereby utilizing the local variation of the refractive index of the medium. The photoinduced changes in polarity and molecular structure have led to widespread applications of azobenzene derivatives as reversible molecular switching devices. Although numerous publications on isomerization of azo dyes have appeared[1−18] recently, still the mechanism of isomerization in general remains a subject of controversy and various research groups are actively involved in addressing this problem. The reason for this controversy is the presence of N lone pair in the azo group. In azo dyes, unlike the well studied isoelectronic stilbene derivatives, there are two possible routes of isomerization,[19] the first involves rotation (torsion or twist) about the central N═N bond which includes a π bond rupture, and the second involves inversion {in-plane (ip) lateral shift} through a linear transition state where the π bond remains intact.

In spite of the vast literature on the studies of the photoisomerization of azo dyes by means of various spectroscopic and photochemical methods including UV−vis absorption,[20−24] infrared (IR),[25] and Raman,[15,16,26−37] the structure of azo dyes are not well established. This is possibly due to the fact that majority of the IR and Raman studies on azo dyes have focused their attention on a qualitative understanding of the vibrational structure and band assignments without paying much attention on the complete normal coordinate analysis, until recently.[17,38−40] In fact, an accurate normal mode analysis is essential in order to understand mode dependent structural distortions involved during the isomerization process.

Density functional theory (DFT) is being widely used for the computation of molecular structure and vibrational frequencies[17,41−57] due to the development of numerous density functional forms and their efficiency which leads to the computation of highly accurate fundamental vibrational frequencies, in addition to modest computational expenses as compared to other sophisticated approaches such as the second-order Moller−Plesset (MP2) perturbation method. In particular, for polyatomic molecules (typically normal modes exceeding 50), the DFT methods lead to the prediction of very accurate molecular structure and vibrational frequencies as compared to the conventional *ab initio* restricted Hartree−Fock (RHF) and MP2 calculations. Computed frequencies using MP2 (compared to RHF) are found to be relatively close to the experimental results, due to the inclusion of electron correlations;[58] however, computationally it is very demanding (in terms of CPU time and disk usage) in comparison to the density functional methods, as a result of which it is restricted for their usefulness to rather small systems. The DFT methods thus provide a promising cost-effective approach for calculating the vibrational spectra of large polyatomic molecules. Interestingly, the DFT calculations are being commonly used these days in order to obtain accurate normal mode descriptions in terms of the potential energy distributions (PEDs) of large polyatomic molecules.[17,41,51,56,57]

In an effort to gain a better understanding of the electronic structure and vibrational properties of the substituted azo dyes,

* To whom correspondence should be addressed. Email: umapathy@ipc.iisc.ernet.in. E-mail: suma@hamsadvani.serc.iisc.ernet.in. Fax: 91-80-3316552.

[†] Present address: Abteilung CD, Hahn Meitner Institute, Glienicker Strasse 100, D-14109, Berlin, Germany.

10.1021/jp9929263 CCC: $19.00
Published on Web 02/25/2000

in the present work, we investigate the Fourier transform infrared (FTIR) and Raman studies of 4-nitro-azobenzene (NAB), 4-(dimethylamino)-azobenzene (DAB), and 4-nitro,4′-(dimethylamino)-azobenzene (NDAB) and also employ density functional theory. The main objective for carrying out the present investigation is 3-fold: (1) An accurate force field is necessary to get vibrational mode dependent information associated with the isomerization dynamics of the substituted azo dyes, from the resonance Raman (RR) intensities.[15,16,59] (2) The normal mode descriptions for NAB, DAB and NDAB are necessary for the accurate assignment of the vibrational spectra,[26−37] and to the best of our knowledge these data are not available in the literature. (3) A critical comparison of the experimentally observed (FTIR and Raman) spectra with the theoretical (DFT) results is absolutely essential in order to test the accuracy of the theory. We present the optimized geometries and the vibrational spectra (including their isotopic analogues) for NAB, DAB, and NDAB employing hybrid (HF/DF) method, viz. B3LYP with 6-31G basis set, since this method is known to predict fundamental frequencies and structural parameters with reasonable accuracy utilizing moderate computational efforts. The results obtained theoretically are critically compared with the experimental FTIR and Raman frequencies. The differences in the vibrational spectra of the substituted azobenzene derivatives in relation to their respective molecular structure and vibrational frequencies are investigated and subsequently compared with the spectra of the parent azo dye, viz. *trans*-azobenzene (TAB).[17,38] For the sake of brevity, throughout this paper we restrict ourselves mainly to the discussion of experimentally observed normal modes.

Computational Details

The DFT calculations presented here were carried out using Gaussian 94 set of programs[60] on an IBM-RS6000 computer system. The molecular geometries of NAB, DAB and NDAB were optimized employing the density functional Becke's three parameter hybrid method[61,62] using the LYP correlation functional[63] (B3LYP) with the 6-31G basis set. This basis set is sufficiently complete in order to permit a good description of the wave function and at the same time it can be extended to larger polyatomic systems with reasonable computational cost.

Berny's optimization algorithm[64] was used to carry out complete geometry optimization for the substituted azobenzene derivatives. The normal modes and vibrational frequencies were then evaluated at the computed equilibrium geometries by analytic evaluation of the second derivatives of energy. The PEDs of the normal modes were calculated by transforming the displacements from the Cartesian to internal coordinate basis using a program NMODES.[57]

Experimental Details

The FTIR spectra were recorded at room temperature in a Bio-Rad FTS-7 spectrophotometer using KBr pellete. The excitation wavelength, viz. 630 nm, for the Raman experiment was scanned using a tunable laser pulse output from an optical parametric oscillator (OPO) (MOPO 730, Spectra Physics). The OPO was pumped by the third harmonic (355 nm) of a 10 Hz Q-switched, Nd:YAG laser (GCR 250, Spectra Physics) providing a high energy laser pulse of 560 mJ. The energy of the OPO output was in the range of 4−8 mJ/pulse. A SPEX 1404 double monochromator was used with two 600 groove gratings blazed at 500 nm to disperse the scattered light. A liquid nitrogen cooled charge coupled device (Princeton Instruments) with 576 × 378 pixels was used as the multichannel detector. The recorded Raman spectra were calibrated using known solvent bands as reference, and the spectral resolution was estimated to be 5 cm^{-1}.

NDAB was prepared by the coupling reaction of *p*-nitrobenzene-diazonium-tetrafluoroborate with *N*,*N*-dimethyl-aniline at 3−5 °C[65] and was purified by column chromatography, on acidified alumina with toluene as eluent followed by recrystallization from toluene.[65] Carbon tetrachloride (CCl_4) was of analytical grade and used as received. NAB and DAB were purchased from Aldrich Chemical Co. and used as received. For the Raman measurements, the solutions of NAB, DAB, and NDAB in CCl_4 were circulated through a capillary at the rate of about 10 mL/min to avoid local heating during exposure, and the scattered light was collected using a 90° scattering geometry.

Results and Discussion

Geometrical Structures. The geometrical structures of NAB, DAB, and NDAB were optimized using hybrid HF/DF method, viz. B3LYP, with 6-31G basis set. During complete geometry optimization, NAB adopted the C_S point group with only a plane of symmetry, whereas, due to the presence of the dimethylamino group in DAB and NDAB, these adopted the C_1 point group containing no symmetry element. The molecular structures of NAB, DAB, and NDAB, and their atom numbering are depicted in Figure 1a−c. The optimized parameters, i.e., bond lengths and bond angles of NAB, DAB, and NDAB computed using B3LYP with the 6-31G basis set are presented in Table 1 along with the calculated[17] and experimental[66] structural parameters of TAB. To the best of our knowledge, this is the first report on the molecular structural parameters of these important class of molecules, viz. NAB, DAB, and NDAB. For the sake of brevity, only the average optimized parameters are presented in Table 1. As seen in the table, the calculated average bond lengths, viz. N═N, C−N, C−C, and C−H, and bond angles, viz. C−N═N and C−C−N, from B3LYP/6-31G in the case of TAB are comparable to the electron diffraction (ED) results. This gives us additional confidence that the B3LYP/6-31G calculation predicts optimized structural parameters in good agreement with the experiment. The knowledge of the differences between ED and the theoretically calculated optimized structures are essential when experimental structural parameters are not available and one has to rely completely on the calculated parameters. Thus, with the information that B3LYP/6-31G is capable of predicting reliably good optimized structures, we present a comparative study of the N═N, C−N, C−C, and C−H bond lengths as well as C−N═N and C−C−N bond angles in TAB, NAB, DAB, and NDAB. From the table, it is found that, upon substitution of the parent TAB molecule by an electron acceptor (nitro group in NAB), electron donor (*N*,*N*-dimethylamino group in DAB), and electron donor−acceptor (in NDAB), the N═N bond distance increases from 1.278 to 1.279, 1.284, and 1.289 Å, respectively. Similarly, the C−C bond distance although remains the same in NAB as compared to TAB, but increases in DAB and NDAB by 0.004 and 0.005 Å, respectively. Interestingly, a reverse trend is observed for the C−N(azo) bond distance. The C−N(azo) bond length decreases by 0.002, 0.007, and 0.014 Å in NAB, DAB, and NDAB, respectively, as compared to TAB. The C−H bond lengths are almost similar in TAB and all its substituted analogues. In NDAB, there is a shortening in C(Ph)−N(NO) bond length by 0.002 Å and an increase in N−O bond distance by 0.001 Å as compared to NAB. Similarly, in NDAB relative to DAB, the C(Ph)−N(Me) and C−H(Me) bond distances

TABLE 1: Optimized Geometrical Parameters of Substituted Azobenzenes in Its Ground State

	NAB	DAB	NDAB	TAB	
bond lengths (Å)	B3LYP/6-31G	B3LYP/6-31G	B3LYP/6-31G	B3LYP/6-31G	ED[a]
N═N	1.279	1.284	1.289	1.278	1.268
C−N (azo)	1.422	1.417	1.410	1.424	1.427
C−C	1.402	1.406	1.407	1.402	1.396
C−H	1.084	1.084	1.083	1.084	1.088
C(Ph)−N(NO)	1.461		1.459		
N−O	1.266		1.267		
C(Ph)−N(Me)		1.386	1.380		
C−H (Me)		1.096	1.095		
C(Me)−N		1.464	1.466		
bond angles (deg)					
C(Ph)−N═N	115.7	115.9	115.7	115.7	114.5
C(Ph)−C(Ph)−N1(azo)	124.3	124.8	124.8	124.3	123.0
C(Ph)−C(Ph)−N2(azo)	115.3	115.9	115.9	115.4	
C(Ph)−C(Ph)−C(Ph)	120.2	119.9	120.1	119.9	
C(Ph)−C(Ph)−H	119.5	119.1	119.2	119.9	
C−C−N(NO)	119.4		119.0		
C−N−O	118.1		118.2		
C−C−N(Me)		121.2	121.2		
C−N−C(Me)		120.3	120.4		
N−C−H(Me)		110.9	110.8		

[a] Reference 66.

decrease by 0.006 and 0.001 Å, and the C(Me)−N bond length undergoes an increase of 0.002 Å. Thus, the contraction of the C−N(azo) bond and the expansion of the N═N and C−C bonds in the substituted azo dyes as compared to those in TAB indicate a greater conjugation and π-electron delocalization. The calculated C−N═N bond angle is found to be the same for TAB, NAB, and NDAB and shows an increase of 0.2° in the case of DAB, while C−C−N1(azo) and C−C−N2(azo) bond angles, although being almost similar for TAB and NAB, show an increase of 0.5° in DAB and NDAB. The C−C−C bond angle increases by 0.3° and 0.2° in NAB and NDAB but remains the same in DAB as compared to that in TAB. A comparison of the C−C−H bond angles relative to TAB shows a decrease of 0.4°, 0.8°, and 0.7° in NAB, DAB, and NDAB, respectively. In NDAB, the C−C−N(NO) bond angle is reduced by 0.4° as compared to that in NAB and suffers an increase in C−N−O bond angle by 0.1°. Similarly, as compared to that in DAB, the C−C−N(Me) bond angle remains the same in NDAB while the C−N−C(Me) bond angle increases by 0.1° and the N−C−H(Me) bond angle decreases by 0.1°.

Fundamental Frequencies of NAB. NAB is composed of 26 atoms, as a result of which it contains 72 normal vibrations. Since the molecule belongs to the C_S point group, the 72 fundamental vibrations can be distributed as 49A′+23A″. All the fundamental modes are both infrared (IR) and Raman active. A′ and A″ type vibrations can be identified only when they are resolved through the depolarization ratio of Raman intensity, since A′ and A″ type modes are expected to be polarized and depolarized, respectively, in the Raman spectrum. Due to the unavailability of the depolarization ratios for NAB, both A′ and A″ species are assigned to the same band wherever the calculated frequencies lie very close to each other.

Assignment of the Spectra. The FTIR spectrum of NAB is shown in Figure 2a, while in Figure 2b is displayed its Raman spectrum measured at 630 nm excitation. The FTIR spectrum shows a number of bands appearing at 1607, 1590, 1523, 1487, 1467, 1443, 1408, 1343, 1303, 1216, 1180, 1161, 1143, 1103, 1072, 999, 969, 928, 861, 825, 810, 775, 752, 722, 689, 633, 614, 586, 541, 506, 462, and 417 cm^{-1}. Similarly, the Raman bands of NAB are observed at 1602, 1495, 1473, 1449, 1413, 1380, 1348, 1314, 1180, 1143, 1109, 1000, 928, 861, 827, 808, 728, 695, 611, and 528 cm^{-1}. It is observed from Figure 2b that the most intense Raman fundamentals of NAB appear at 1143, 1449, 1473, 1495, 1602, 1348, 1180, 1413, and 1109 cm^{-1}, followed by a few weak modes at 1000, 1314, 1380, 928, 861, 611, 528, 695, 728, 808, and 827 cm^{-1}. The calculated IR spectrum is also shown in Figure 2a. A Lorentzian broadening of 7 cm^{-1} is employed in order to plot the spectrum. A comparison of the calculated and observed IR spectra shows good agreement. Thus, the observed IR active fundamentals can be assigned more reliably on the basis of a comparison of the IR intensities along with the computed wavenumbers. The computed (unscaled) frequencies as well as the PEDs of various vibrational modes of NAB along with the experimentally observed FTIR and Raman frequencies are listed in Table 2. The frequencies as well as the PEDs of vibrations which are not observed experimentally are available as Supporting Information, Table S1. The calculated frequencies for the experimentally observed A′ and A″ vibrations for the isotopomers of NAB, viz. $C_6H_5N_1{}^{15}N_2C_6H_4NO_2$, $C_6H_5N_1N_2{}^{15}C_6H_4NO_2$, and $C_6H_5N_1{}^{15}N_2{}^{15}C_6H_4NO_2$, are given in Table 3 along with its IR intensities while the results from all other vibrations are available as Supporting Information, Table S2. For NAB, since no experimental data is available for any isotope, our discussion is mainly confined to the theoretically computed frequencies for the in-plane (ip) and out-of-plane (oop) vibrations and the calculated shifts observed for the isotopomers. Since, NAB is planar, it is found that there is no mixing of the ip and oop vibrations. All the vibrations corresponding to A′ symmetry are ip active while those belonging to A″ symmetry are oop active.

In-Plane (ip) Vibrations of NAB. Among the 49 ip active vibrations, 12A′ fundamentals, viz. $\upsilon_{10}-\upsilon_{12}$, υ_{14}, υ_{15}, υ_{19}, υ_{22}, υ_{27}, υ_{28}, υ_{31}, υ_{32}, and υ_{41}, correspond to the C−C stretch and are coupled to ip C−C/C−H/C−N bending modes with additional coupling from various other vibrations. Due to the low molecular symmetry in NAB, it is observed from the PEDs in Table 2 that these skeletal C−C stretching vibrations are highly mixed with the C−C and C−H ip bending modes. Two vibrations of A′ symmetry, υ_{20} and υ_{21}, are assigned purely to the C−C stretch. The C−C stretching vibrations, υ_{10}, υ_{11}, υ_{12}, υ_{14}, υ_{15}, υ_{19}, υ_{27}, υ_{28}, υ_{31}, υ_{32}, and υ_{41}, are observed in the FTIR spectrum at 1607, 1523, 1590, 1487, 1467, 1408, 1180, 1161, 1103, 1072, and 928 cm^{-1}, and υ_{10}, υ_{14}, υ_{15}, υ_{19}, υ_{22}, υ_{27}, υ_{31},

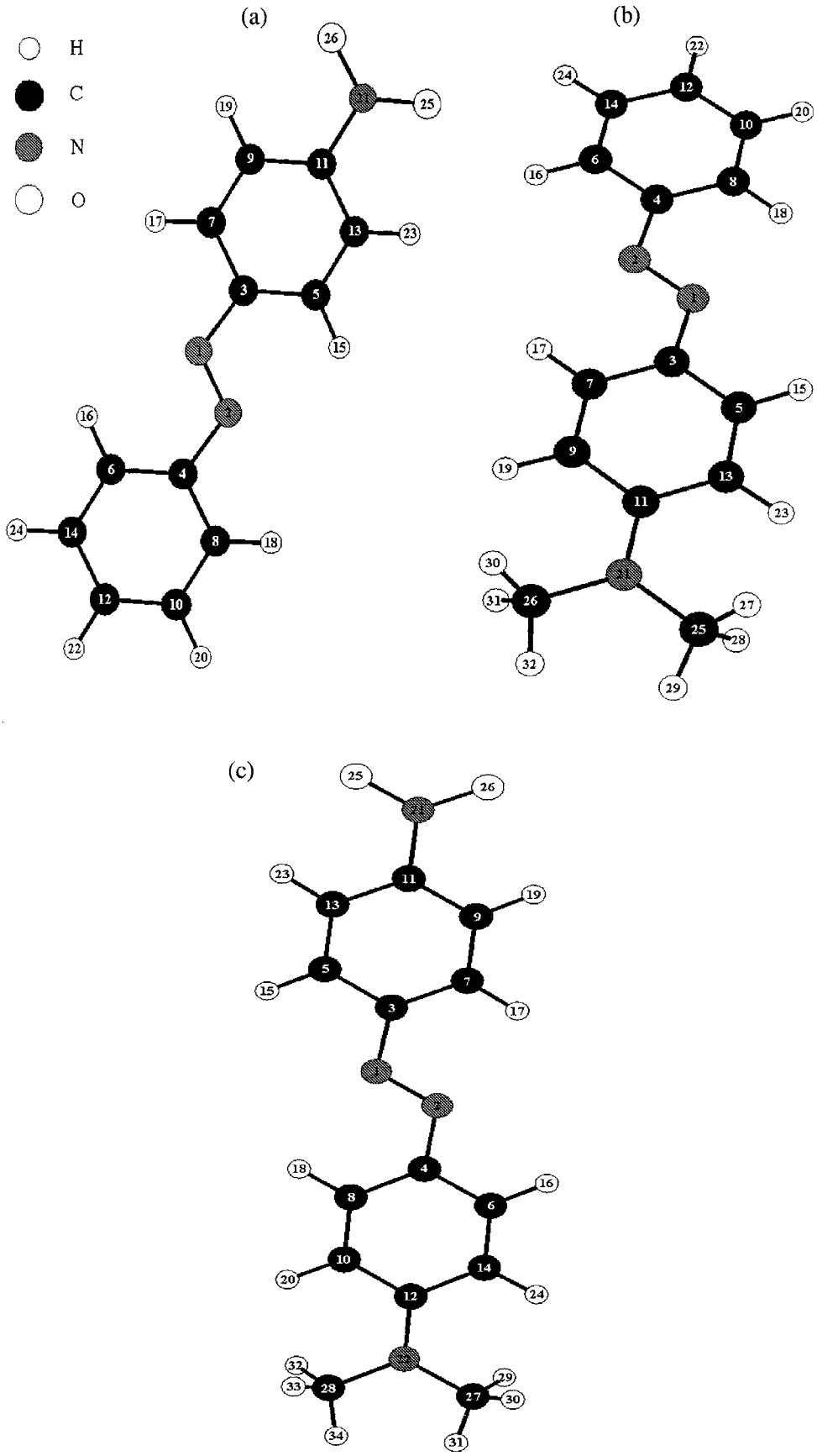

Figure 1. The optimized geometry and atom numbering of (a) 4-nitro-azobenzene, (b) 4-(dimethylamino)-azobenzene, and (c) 4-nitro,4′-(dimethylamino)-azobenzene.

and υ_{41} appear in the Raman spectrum at 1602, 1495, 1473, 1413, 1314, 1180, 1109, and 928 cm^{-1}. Upon substitution of either or both the azo N atoms by N,[15] most of the C−C stretching vibrations undergo almost no change or very little change (i.e., 1 or 2 cm^{-1}) with the exception of υ_{19} and υ_{41} which undergo a shift of 13−14−9 and 9−9−19 cm^{-1} ($N_1{}^{15}$-

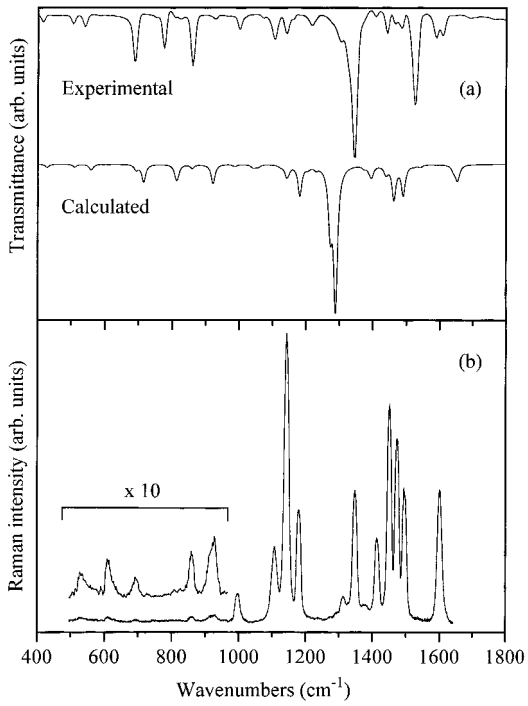

Figure 2. (a) The experimental and calculated FTIR spectra of 4-nitro-azobenzene, and (b) its Raman spectrum in CCl_4 at 630 nm excitation.

$N_2^{15}-N_1^{15}N_2^{15}$), respectively, as shown in Table 3. The calculated azo (N═N) stretch, υ_{18} appears at 1462 cm^{-1} and is coupled to the N−O stretch. The experimentally observed bands corresponding to the N═N stretch appear at 1443 (medium intensity) and 1449 cm^{-1} in the FTIR and Raman spectra, respectively. The azo stretching vibration undergoes a large downshift in frequency of 32, 34, and 50 cm^{-1} due to an increase in the reduced mass, upon N^{15} substitution of N_1, N_2 and both N_1N_2, respectively. The mode υ_{23} appearing at the calculated frequency of 1353 cm^{-1} is assigned to the C−H ip bend and is coupled to the C−N ip bend and the C−C stretch. The experimentally observed FTIR band at 1303 cm^{-1} with weak intensity corresponds to this vibration. The mode υ_{24} corresponds to the N−O stretch and is coupled to the C−N(NO) stretch. An intense band corresponding to the N−O stretch is observed at a substantially higher frequency in the FTIR and Raman spectra at 1343 and 1348 cm^{-1}, as compared to that calculated theoretically using B3LYP with 6-31G basis (1288 cm^{-1}). Two modes, υ_{25} and υ_{29}, appearing at 1272 and 1181 cm^{-1} correspond to the asymmetric and symmetric C−N stretch, respectively. These vibrational modes are coupled to the C−C ip bend and the C−C stretch with additional contribution from the C−N ip bend in the case of υ_{29}. The FTIR band corresponding to the asymmetric C−N stretch appears at 1216 cm^{-1}, whereas, both the FTIR and Raman spectra show a band at 1143 cm^{-1} corresponding to the symmetric C−N stretch. Both of these C−N stretching vibrations are observed in the FTIR spectrum with medium intensity but our calculation predicts strong intensity. These modes shift by 3 and 6 cm^{-1}, respectively, upon N^{15} substitution of either or both the azo N atoms. 4A′ type vibrations, viz. υ_{37}, υ_{49}, υ_{54}, and υ_{60}, are assigned to the C−C ip bend and are coupled to the C−C stretch or C−N ip bend. Of these vibrations, υ_{54} and υ_{60} are observed only in the FTIR spectrum at 586 and 417 cm^{-1}. The modes υ_{37} and υ_{49} are observed both in the FTIR (Raman) spectra at 999 (1000) and 722 (728) cm^{-1}, respectively. The mode υ_{54} undergoes a shift of 2−4−6 cm^{-1} upon N^{15} substitution ($N_1^{15}-N_2^{15}-N_1^{15}N_2^{15}$) due to contribution from the C−N ip bend. Two modes, υ_{52} and υ_{53}, appearing at the computed frequency of 662 and 646 cm^{-1} are assigned purely to the C−C ip bend. Of these vibrations, υ_{52} is observed in the FTIR spectrum (633 cm^{-1} with weak intensity) and υ_{53} appears both in the FTIR (weak intensity) and Raman spectra at 614 and 611 cm^{-1}, respectively. 2A′ vibrations, viz. υ_{56} and υ_{57}, are assigned to the C−N ip bend and are coupled to the C−C/N−O ip bend. Both these vibrations, υ_{56} and υ_{57}, are observed in the Raman and FTIR (medium intensity) spectra at 528 and 506 cm^{-1}, respectively, and undergo a downshift of 2−3−5 and 2−2−5 cm^{-1} upon N^{15} isotopic substitution ($N_1^{15}-N_2^{15}-N_1^{15}N_2^{15}$).

Out-of-Plane (oop) Vibrations of NAB. NAB consists of 23 oop vibrations of A″ symmetry. The modes υ_{43} and υ_{44}

TABLE 2: Calculated Frequencies and the PEDs of 4-Nitro-azobenzene, Obtained from B3LYP/6-31G[a]

		exptl						exptl			
mode	S	FTIR	Raman	B3LYP/6-31G	PED (%)[a]	mode	S	FTIR	Raman	B3LYP/6-31G	PED (%)[a]
ν_{10}	A′	1607	1602	1659	70υ(C−C),19δ(C−C)	ν_{32}	A′	1072		1123	59υ(C−C), 17δ(C−C)
ν_{11}	A′	1523		1652	73υ(C−C),17δ(C−C)						13δ(C−N)
ν_{12}	A′	1590		1642	64υ(C−C),25δ(C−C)	ν_{37}	A′	999	1000	1039	73δ(C−C),22υ(C−C)
ν_{14}	A′	1487	1495	1541	61υ(C−C),19δ(C−H)	ν_{38}	A″	969		1034	68τ(C−C),31γ(C−H)
ν_{15}	A′	1467	1473	1536	60υ(C−C),19δ(C−H)	ν_{41}	A′	928	928	940	38υ(C−C),33δ(C−C)
ν_{18}	A′	1443	1449	1462	45υ(N═N),31υ(N−O)						13υ(C−N),11δ(N═N)
ν_{19}	A′	1408	1413	1438	39υ(C−C),25υ(N−O)	ν_{42}	A″	861	861	921	51τ(C−C),41γ(C−H)
					17υ(N═N)	ν_{43}	A″	825	827	887	99γ(C−H)
ν_{20}	A′		1380	1396	92υ(C−C)	ν_{44}	A″	810	808	883	100γ(C−H)
ν_{22}	A′		1314	1373	34υ(C−C),28δ(C−N)	ν_{47}	A″	775		811	65τ(C−C),29γ(C−H)
					27δ(C−H)	ν_{48}	A″	752		768	87τ(C−C), 10γ(C−H)
ν_{23}	A′	1303		1353	52δ(C−H),23δ(C−N)	ν_{49}	A′	722	728	716	73δ(C−C),12δ(C−N)
					17υ(C−C)	ν_{50}	A″	689	695	714	81τ(C−C),18γ(C−H)
ν_{24}	A′	1343	1348	1288	49υ(N−O),30υ(C−N)$_{NO}$	ν_{52}	A′	633		662	89δ(C−C)
ν_{25}	A′	1216		1272	35υ(C−N),26δ(C−C)	ν_{53}	A′	614	611	646	94δ(C−C)
					22υ(C−C)	ν_{54}	A′	586		607	63δ(C−C),21δ(C−N)
ν_{27}	A′	1180	1180	1226	48υ(C−C),48δ(C−H)	ν_{55}	A″	541		561	72τ(C−C),18γ(C−H)
ν_{28}	A′	1161		1205	33υ(C−C),23δ(C−C)	ν_{56}	A′		528	557	51δ(C−N),33δ(C−C)
					20δ(C−H),16υ(C−N)	ν_{57}	A′	506		510	50δ(C−N),18δ(N−O)
ν_{29}	A′	1143	1143	1181	34υ(C−N),31δ(C−C)						15υ(C−C)
					19υ(C−C),10δ(C−N)	ν_{58}	A″	462		503	68τ(C−C),22γ(C−H)
ν_{31}	A′	1103	1109	1141	38υ(C−C),34δ(C−C)	ν_{60}	A′	417		428	53δ(C−C),16υ(C−N)$_{NO}$
					16υ(C−N)$_{NO}$						13δ(C−N)

[a] υ, stretch; δ, in-plane bend; out-of-plane bend; τ, torsion; S, symmetry.

TABLE 3: Calculated Frequencies for Isotopic Derivatives of 4-Nitro-azobenzene, Obtained from B3LYP/6-31G

		$C_{12}H_9N_1N_2NO_2$				$C_{12}H_9N^{15}{}_1N_2NO_2$		$C_{12}H_9N_1N^{15}{}_2NO_2$		$C_{12}H_9N^{15}{}_1N^{15}{}_2NO_2$	
mode	character	FTIR	Raman	calcd	I^a	calcd	I^a	calcd	I^a	calcd	I^a
ν_{10}	υ(C−C)	1607m	1602	1659	8.2	1659	6.8	1659	6.9	1658	5.9
ν_{11}	υ(C−C)	1523s		1652	45.6	1652	48.5	1651	48.8	1651	51.0
ν_{12}	υ(C−C)	1590m		1642	11.2	1642	12.5	1642	13.8	1642	14.6
ν_{14}	υ(C−C)	1487m	1495	1541	7.2	1540	6.0	1541	7.7	1540	6.7
ν_{15}	υ(C−C)	1467w	1473	1536	0.3	1535	0.0	1535	0.0	1535	0.1
ν_{18}	υ(N═N)	1443m	1449	1462	105.7	1430	50.2	1428	46.8	1412	58.7
ν_{19}	υ(C−C)	1408w	1413	1438	26.8	1451	67.0	1452	73.0	1447	44.7
ν_{20}	υ(C−C)		1380	1396	27.6	1396	28.3	1395	26.4	1396	25.9
ν_{22}	υ(C−C)		1314	1373	8.7	1372	12.5	1373	8.7	1371	14.7
ν_{23}	δ(C−H)	1303w		1353	0.2	1353	0.2	1352	0.3	1352	0.7
ν_{24}	υ(N−O)	1343s	1348	1288	433.7	1287	473.3	1287	466.3	1287	494.1
ν_{25}	υ(C−N)	1216m		1272	181.5	1269	142.5	1269	146.9	1266	120.3
ν_{27}	υ(C−C)	1180w	1180	1226	0.5	1226	0.3	1226	0.2	1226	0.2
ν_{28}	υ(C−C)	1161w		1205	9.0	1204	11.9	1204	6.8	1203	9.7
ν_{29}	υ(C−N)	1143m	1143	1181	94.1	1178	85.2	1178	96.6	1175	87.9
ν_{31}	υ(C−C)	1103m	1109	1141	32.1	1141	33.8	1141	33.4	1141	35.2
ν_{32}	υ(C−C)	1072w		1123	5.1	1123	5.1	1123	5.0	1123	5.0
ν_{37}	δ(C−C)	999m	1000	1039	6.2	1039	6.2	1038	6.4	1038	6.4
ν_{38}	τ(C−C)	969w		1034	0.2	1034	0.2	1034	0.2	1034	0.2
ν_{41}	υ(C−C)	928w	928	940	0.3	931	0.5	931	0.5	921	0.9
ν_{42}	τ(C−C)	861s	861	921	60.4	921	60.4	921	60.4	921	60.3
ν_{43}	γ(C−H)	825w	827	887	1.0	887	1.0	887	1.0	887	1.0
ν_{44}	γ(C−H)	810sh	808	883	0.0	883	0.0	883	0.0	883	0.0
ν_{47}	τ(C−C)	775s		811	31.0	811	31.2	811	31.2	811	31.4
ν_{48}	τ(C−C)	752w		768	1.1	768	1.0	768	1.1	768	1.0
ν_{49}	δ(C−C)	722sh	728	716	9.0	714	9.3	715	8.8	714	9.0
ν_{50}	τ(C−C)	689s	695	714	46.4	714	46.3	714	46.4	714	46.3
ν_{52}	δ(C−C)	633w		662	0.5	661	0.5	661	0.4	661	0.4
ν_{53}	δ(C−C)	614w	611	646	0.5	646	0.5	646	0.5	646	0.5
ν_{54}	δ(C−C)	586w		607	1.8	605	1.7	603	1.8	601	1.7
ν_{55}	τ(C−C)	541m		561	9.0	560	9.1	560	9.0	559	9.1
ν_{56}	δ(C−N)		528	557	10.4	555	9.2	554	9.2	552	8.1
ν_{57}	δ(C−N)	506m		510	9.2	508	9.9	508	9.9	505	10.5
ν_{58}	τ(C−C)	462w		503	0.0	503	0.0	503	0.0	503	0.0
ν_{60}	δ(C−C)	417m		428	10.7	427	10.7	427	10.9	426	10.8

[a] *I* represents the infrared intensities in km/mol sh, shoulder; m, medium; s, strong; w, weak.

correspond purely to the C−H oop bend. These 2A″ type vibrations are observed in the FTIR (Raman) spectra at 825 (827) and 810 (808) cm^{-1}, and undergo no change in frequency upon N^{15} substitution. 7A″ type vibrations, υ_{38}, υ_{42}, υ_{47}, υ_{48}, υ_{50}, υ_{55}, and υ_{58}, are assigned to the C−C torsion and are coupled to the C−H oop bend. The modes υ_{42} and υ_{50} are observed experimentally both in the FTIR (Raman) spectra at 861 and 689 (695) cm^{-1}, whereas υ_{38}, υ_{47}, υ_{48}, υ_{55}, and υ_{58} are observed only in the FTIR spectrum at 969, 775, 752, 541, and 462 cm^{-1}. An overall one-to-one correspondence between the calculated (using B3LYP with 6-31G basis) and the experimental frequencies is observed for the ip and oop vibrations of NAB. Even the computed and the experimental IR intensities as displayed in Table 3 and Figure 2a show reasonable agreement with the exception of a few vibrations, υ_{18}, υ_{19}, υ_{25}, and υ_{29} where the observed and calculated intensities appear as medium and strong, respectively.

Fundamental Frequencies of DAB. DAB consists of 32 atoms and hence it has 90 fundamental vibrations. Trying to restrict the molecule within a plane resulted in two imaginary frequencies. Thus, no symmetry restriction was applied during geometry optimization. Since the molecule has no element of symmetry, all the fundamental modes are both IR and Raman active.

Assignment of the Spectra. The FTIR spectrum of DAB as shown in Figure 3a contains a number of vibrational bands appearing at 1605, 1560, 1517, 1483, 1458, 1443, 1408, 1370, 1311, 1231, 1194, 1154, 1138, 1065, 1016, 946, 916, 826, 822, 762, 721, 684, 638, 544, 514, 489, 469, and 428 cm^{-1}. In Figure 3b is shown the Raman spectrum of DAB obtained at 630 nm excitation. The Raman fundamentals of DAB are observed at

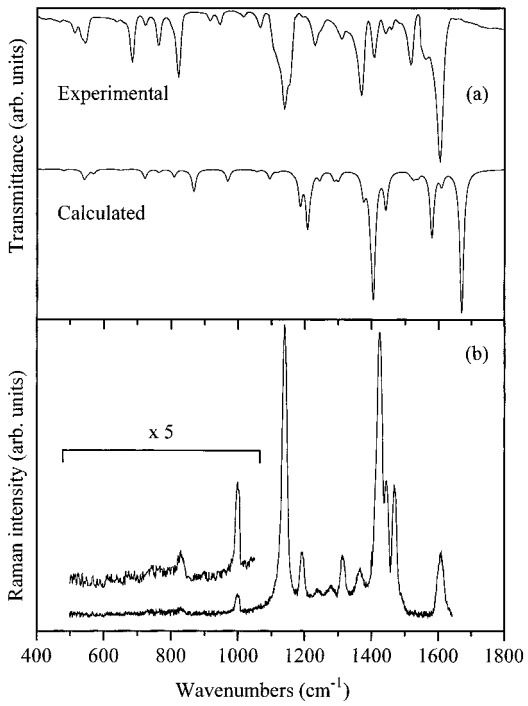

Figure 3. (a) The experimental and calculated FTIR spectra of 4-(dimethylamino)-azobenzene, and (b) its Raman spectrum in CCl_4 at 630 nm excitation.

TABLE 4: Calculated Frequencies and the PEDs of 4-Dimethylamino-azobenzene, Obtained from B3LYP/6-31G

	exptl					exptl			
mode	FTIR	Raman	B3LYP/6-31G	PED (%)[a]	mode	FTIR	Raman	B3LYP/6-31G	PED (%)[a]
ν_{16}	1605	1608	1670	71υ(C−C),18δ(C−C)	ν_{46}	1065		1117	59υ(C−C),18δ(C−C) 14δ(C−N)
ν_{18}	1560		1639	64υ(C−C),26δ(C−C)					
ν_{20}	1517		1580	35υ(C−C),25υ($C_{Ph}-N_{Me}$) 13δ(C−C)	ν_{48}	1016		1056	48δ(C−C),47υ(C−C)
					ν_{51}		998	1035	71δ(C−C),23υ(C−C)
ν_{25}	1483		1526	71$\tau$$(C-N)_{Me}$,22$\delta$$(C-H)_{Me}$	ν_{55}	946		972	49γ(C−H),48τ(C−C)
ν_{27}		1470	1516	44υ(C−C),22δ(C−N) 14δ(C−C),14δ(C−H)	ν_{57}	916		940	51υ(C−C),34δ(C−C) 10δ(N═N)
ν_{28}	1458		1501	63υ(C−C)	ν_{59}	822	831	867	53τ(C−C),32γ(C−H) 11$\tau$$(C-N)_{Me}$
ν_{29}	1443	1444	1490	39υ(C−C),26$\delta$$(C-H)_{Me}$ 12δ(C−N)	ν_{60}	826	831	852	51δ(C−C),46υ(C−C)
ν_{30}	1408	1423	1442	65υ(N═N),11δ(C−N)	ν_{62}	762		808	65τ(C−C),30γ(C−H)
ν_{32}	1370	1367	1396	74υ(C−C)	ν_{63}		747	763	85τ(C−C)
ν_{35}	1311	1314	1371	48υ(C−C),29δ(C−N) 18δ(C−H)	ν_{64}	721		755	48δ(C−C),15υ(C−C) 15δ(C−N),13$\upsilon$$(C-N)_{Me}$
ν_{36}	1231	1239	1300	34υ(C−N),26υ(C−C) 26δ(C−C)	ν_{65}	684		721	82τ(C−C),16γ(C−H)
					ν_{66}		669	670	87δ(C−C)
ν_{37}		1279	1287	49$\upsilon$$(C-N)_{Me}$,31$\upsilon$(C−C)	ν_{67}	638		651	80δ(C−C)
ν_{40}	1194	1195	1218	45υ(C−C),44δ(C−H)	ν_{69}	544		569	55τ(C−C),29γ(C−H)
ν_{42}	1138	1138	1186	36υ(C−N),24υ(C−C) 24δ(C−C)	ν_{72}	514		525	60τ(C−C),23γ(C−H)
					ν_{73}	489		480	31δ(C−N),21$\delta$$(C-N)_{Me}$ 17υ(C−C),12δ(C−C)
ν_{43}	1154		1166	52υ(C−C),15δ(C−C) 12δ(C−H),10δ(C−N)	ν_{74}	469		456	91τ(C−C)
					ν_{75}	428		431	95τ(C−C)

[a] υ, stretch; δ, in-plane bend; δ, out-of-plane bend; τ, torsion.

1608, 1470, 1444, 1423, 1367, 1314, 1279, 1239, 1195, 1138, 998, 831, 747, and 669 cm^{-1}. It is observed from the figure that the intense Raman bands appear at 1138 and 1424 cm^{-1}, followed by 1444, 1470, 1608, 1195, 1314, 1367, and 998 cm^{-1}. A few weak bands are observed at 1279, 1239, 831, 747, and 669 cm^{-1}. The calculated IR spectrum convoluted with a lorenzian of line width 7 cm^{-1} is also plotted in Figure 3a. A good agreement is observed between the experimental and calculated spectra. The infrared bands are thus, assigned on the basis of FTIR intensities. The computed (unscaled) frequencies as well as the PEDs of various vibrational modes of DAB along with the experimentally observed FTIR and Raman frequencies are listed in Table 4. The frequencies of vibrations which are not observed experimentally and their PEDs are available as Supporting Information, Table S3. The calculated frequencies for the experimentally observed vibrations of the isotopomers of DAB, viz. $C_6H_5N_1{}^{15}N_2C_6H_4N(CH_3)_2$, $C_6H_5N_1N_2{}^{15}C_6H_4N(CH_3)_2$, and $C_6H_5N_1{}^{15}N_2{}^{15}C_6H_4N(CH_3)_2$, are displayed in Table 5 along with the calculated IR intensities while the results from all other vibrations are available as Supporting Information, Table S4. For all the isotopes of DAB, the IR spectrum is reported.[25] Hence, our discussion is mainly based on a comparison of the theoretically calculated isotopic shifts with those of the experimentally reported[25] ones. Due to the nonplanarity in the structure of DAB, there is considerable mixing of the ip and oop modes.

In DAB, the vibrations υ_{18}, υ_{20}, υ_{27}, υ_{29}, υ_{35}, υ_{40}, υ_{43}, υ_{46}, and υ_{57} are assigned to the C−C stretch and are coupled to the C−C/C−H/C−N ip bend with additional contribution from various other vibrations. As seen from Table 4, the vibrations υ_{28} and υ_{32} are assigned purely to the C−C stretch. For these high-frequency vibrations of DAB, no mixing of the ip and oop modes are observed. Of the various C−C stretching vibrations, five modes, viz. υ_{16}, υ_{29}, υ_{32}, υ_{35}, and υ_{40}, are observed both in the FTIR (Raman) spectra at 1605 (1608), 1443 (1444), 1370 (1367), 1311 (1314), and 1194 (1195) cm^{-1}. Six of the C−C stretching modes, υ_{18}, υ_{20}, υ_{28}, υ_{43}, υ_{46}, and υ_{57} are observed only in the FTIR spectrum at 1560, 1517, 1458, 1154, 1065 and 916 cm^{-1} while, only the mode υ_{27} is observed in the Raman spectrum at 1470 cm^{-1}. The computed and experimental IR intensities as observed in Table 5 and Figure 3a reflect excellent agreement. The modes υ_{35} and υ_{57} show a considerable shift of 2−1−4 and 9−8−18 cm^{-1}, respectively, upon isotopic substitution ($N_1{}^{15}-N_2{}^{15}-N_1{}^{15}N_2{}^{15}$). The vibration, υ_{25} is assigned to the methyl C−N torsion and is coupled to the methyl C−H ip bend. It is observed at 1483 cm^{-1} in the FTIR spectrum with weak intensity, as expected from calculation. The observed PEDs, as displayed in Table 4, show considerable mixing of the oop and ip vibrations in υ_{25}. The mode υ_{30} appearing at the computed frequency of 1442 cm^{-1} corresponds to the N═N stretch and is coupled to the C−N ip bend. The azo stretch is observed at 1408 (medium intensity) and 1423 cm^{-1} in the FTIR and Raman spectra. The azo stretching vibration, upon N^{15} substitution ($N_1{}^{15}-N_2{}^{15}-N_1{}^{15}N_2{}^{15}$), undergoes a shift in the calculated frequency of 18−18−32 cm^{-1}, which is in reasonable agreement with the experimentally observed shift[25] in the IR frequency (1410 cm^{-1}) of 14−14−35 cm^{-1}. The vibrations υ_{36} and υ_{42} are assigned to the asymmetric and symmetric C−N stretch and are coupled to the C−C stretch and the C−C ip bend. The asymmetric C−N stretch is observed in the FTIR and Raman spectra at 1231 and 1239 cm^{-1}, while the symmetric C−N stretch is observed in the FTIR and Raman spectra at 1138 cm^{-1}. The computed and observed IR intensity is medium and strong for the asymmetric and symmetric C−N stretching vibrations. The calculated N^{15} isotopic shifts ($N_1{}^{15}-N_2{}^{15}-N_1{}^{15}N_2{}^{15}$) for these asymmetric and symmetric C−N stretching vibrations are 4−3−6 and 3−4−6 cm^{-1}, respectively, while that reported by Kübler et al.[25] for the latter is 2−3−5 cm^{-1} which is in agreement with our results. The mode υ_{37} corresponds to the methyl C−N stretch and is coupled to the C−C stretch. It undergoes no change in frequency upon N^{15} isotopic substitution and is observed in the Raman spectrum at 1279 cm^{-1}. The fundamentals, υ_{48}, υ_{51}, υ_{60}, and υ_{64} are assigned to the C−C ip bend with coupling from the C−C stretch. The modes υ_{66} and υ_{67} are assigned purely to the C−C ip bend. All these vibrations, assigned to the C−C ip bend, have no mixing from the oop modes. The vibrations υ_{48}, υ_{64}, and υ_{67} are observed only in the FTIR spectrum and they appear at 1016, 721, and 638 cm^{-1}, while υ_{51} and υ_{66} appear in the Raman spectrum at 998 and 669 cm^{-1}. The vibrations, υ_{60}, υ_{64}, and υ_{71} undergo a

TABLE 5: Calculated Frequencies for Isotopic Dervatives of 4-Dimethylamino-azobenzene, Obtained from B3LYP/6-31G

		$C_{12}H_9N_1N_2NC_2H_6$				$C_{12}H_9N^{15}{}_1N_2NC_2H_6$		$C_{12}H_9N_1N^{15}{}_2NC_2H_6$		$C_{12}H_9N^{15}{}_1N^{15}{}_2NC_2H_6$	
mode	character	FTIR	Raman	calcd	I^a	calcd	I^a	calcd	I^a	calcd	I^a
ν_{16}	υ(C−C)	1605s	1608	1670	500.4	1669	507.6	1669	510.6	1669	515.5
ν_{18}	υ(C−C)	1560w		1639	1.6	1638	1.7	1638	1.9	1638	1.9
ν_{20}	υ(C−C)	1517s		1580	232.6	1580	231.6	1580	227.4	1580	227.5
ν_{25}	τ(C−N)$_{Me}$	1483sh		1526	0.0	1526	0.0	1526	0.0	1526	0.0
ν_{27}	υ(C−C)		1470	1516	10.3	1516	8.0	1515	7.6	1514	6.9
ν_{28}	υ(C−C)	1458w		1501	0.6	1501	0.2	1501	0.2	1500	0.2
ν_{29}	υ(C−C)	1443w	1444	1490	0.9	1489	0.3	1490	0.4	1489	0.3
ν_{30}	υ(N═N)	1408m	1423	1442	125.2	1424	36.9	1424	58.9	1410	57.1
ν_{32}	υ(C−C)	1370s	1367	1396	94.0	1396	99.5	1396	99.8	1395	141.8
ν_{35}	υ(C−C)	1311w	1314	1371	0.7	1369	17.6	1370	8.9	1367	145.1
ν_{36}	υ(C−N)	1231m	1239	1300	31.4	1296	28.1	1297	21.9	1294	19.4
ν_{37}	υ(C−N)$_{Me}$		1279	1287	30.6	1286	30.3	1287	30.3	1286	29.5
ν_{40}	υ(C−C)	1194w	1195	1218	1.9	1218	2.3	1218	2.2	1218	2.8
ν_{42}	υ(C−N)	1138s	1138	1186	111.6	1183	135.9	1182	97.8	1180	117.6
ν_{43}	υ(C−C)	1154sh		1166	6.0	1166	6.1	1166	7.7	1166	9.9
ν_{46}	υ(C−C)	1065w		1117	7.9	1117	7.6	1117	7.7	1117	7.4
ν_{48}	δ(C−C)	1016w		1056	6.7	1056	6.5	1056	6.8	1056	6.5
ν_{51}	δ(C−C)		998	1035	0.2	1035	0.3	1035	0.3	1035	0.3
ν_{55}	γ(C−H)	946w		972	5.7	972	5.7	971	5.6	971	5.6
ν_{57}	υ(C−C)	916w		940	0.5	931	0.4	932	0.6	922	0.5
ν_{59}	τ(C−C)	826s	831	867	77.3	866	77.2	867	77.2	866	77.1
ν_{62}	τ(C−C)	762m		808	26.8	808	27.1	807	27.0	807	27.3
ν_{63}	τ(C−C)		747	763	10.0	763	9.8	763	9.9	763	9.7
ν_{64}	δ(C−C)	721w		755	0.9	752	0.8	755	0.9	752	0.9
ν_{65}	τ(C−C)	684s		721	32.8	721	32.8	721	32.8	721	32.8
ν_{66}	δ(C−C)		669	670	1.5	669	1.4	669	1.5	669	1.3
ν_{67}	δ(C−C)	638w		651	3.5	651	3.6	650	2.1	650	2.1
ν_{69}	τ(C−C)	544m		569	13.8	569	13.9	568	13.8	568	13.9
ν_{72}	τ(C−C)	514w		525	0.0	525	0.0	524	0.0	524	0.0
ν_{73}	δ(C−N)	489w		480	5.0	478	5.3	479	5.4	477	5.7
ν_{74}	τ(C−C)	469w		456	0.0	455	0.0	456	0.0	455	0.0
ν_{75}	τ(C−C)	428w		431	0.0	431	0.0	431	0.0	431	0.0

[a] *I* represents the infrared intensities in km/mol sh, shoulder; m, medium; s, strong, w, weak.

downshift in frequency of 3−5−7, 3−0−3 and 3−3−6 cm^{-1} when either or both the N atoms of the azo group is isotopically substituted with N^{15} ($N_1{}^{15}$−$N_2{}^{15}$−$N_1{}^{15}N_2{}^{15}$). The vibrations, υ_{59}, υ_{62}, υ_{65}, υ_{69}, and υ_{72} are assigned to the C−C torsion and have contributions from the C−H oop bending modes. Similarly, the fundamentals υ_{63}, υ_{74}, and υ_{75} are assigned purely to the C−C torsion. A few of these modes assigned to the C−C torsion, viz. υ_{62}, υ_{65}, υ_{69}, υ_{72}, υ_{74}, and υ_{75} appear in the FTIR spectrum at 762, 684, 544, 514, 469, and 428 cm^{-1}, whereas υ_{63} appears in the Raman spectrum at 747 cm^{-1}. The mode υ_{59} is observed both in the FTIR and Raman spectra at 822 (intense band) and 831 cm^{-1}, respectively. For all these IR bands, the calculated and experimental intensities are in reasonable agreement. The mode υ_{55} is assigned to the C−H oop bend and is coupled to the C−C torsion. It appears in the FTIR spectrum at 946 cm^{-1} with low intensity as predicted by our calculation. The vibration υ_{73} is assigned to the C−N ip bend and is coupled to the methyl C−N, C−C ip bends, and the C−C stretch. It is observed in the FTIR spectrum at 489 cm^{-1} and also undergoes a change in frequency of 2−1−3 cm^{-1} upon N^{15} substitution ($N_1{}^{15}$−$N_2{}^{15}$−$N_1{}^{15}N_2{}^{15}$). An overall comparison of the calculated and experimental frequencies as well as infrared intensities show a good agreement in the case of DAB.

Fundamental Frequencies of NDAB. NDAB contains 34 atoms, as a result of which it has 96 fundamental vibrations. As mentioned earlier in the case of DAB, trying to restrict the molecule within a plane resulted in two imaginary frequencies. Hence, no symmetry restriction was applied during geometry optimization. Thus, all the fundamental vibrations in NDAB are both IR and Raman active due to the lack of any element of symmetry.

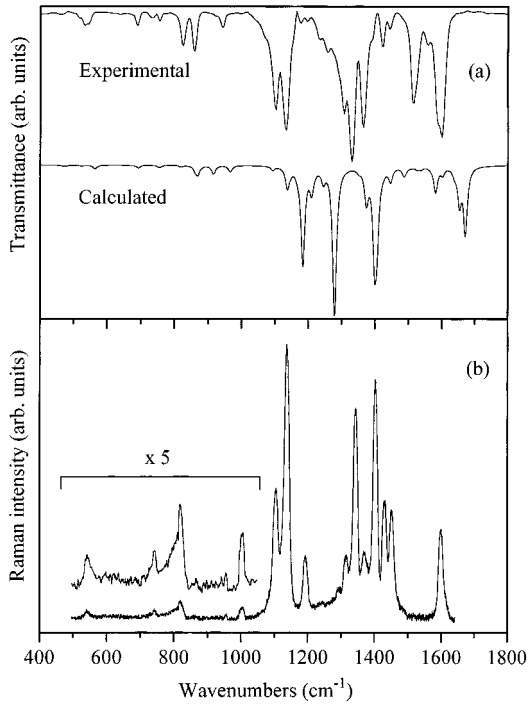

Figure 4. (a) The experimental and calculated FTIR spectra of 4-nitro,4′-(dimethylamino)-azobenzene, and (b) its Raman spectrum in CCl_4 at 630 nm excitation.

Assignment of the Spectra. The FTIR spectrum of NDAB as shown in Figure 4a has various fundamental vibrations appearing at 1601, 1590, 1557, 1515, 1484, 1442, 1422, 1390, 1364, 1331, 1307, 1259, 1234, 1198, 1177, 1133, 1101, 1068,

TABLE 6: Calculated Frequencies and the PEDs of 4-Nitro,4′-dimethylamino-azobenzene, Obtained from B3LYP/6-31G

	exptl					exptl			
mode	FTIR	Raman	B3LYP/6-31G	PED (%)[a]	mode	FTIR	Raman	B3LYP/6-31G	PED (%)[a]
ν_{15}	1601	1595	1671	71υ(C−C),18δ(C−C)	ν_{51}	1000	1002	1034	75δ(C−C),20υ(C−C)
ν_{16}	1590		1653	69υ(C−C),19δ(C−C)	ν_{53}	975		1029	66τ(C−C),32γ(C−H)
ν_{17}	1557		1638	64υ(C−C),25δ(C−C)	ν_{54}	960	955	1003	66τ(C−C),32γ(C−H)
ν_{19}	1515		1581	37υ(C−C),23υ(C_{Ph}−N_{Me}) 17δ(C−C)	ν_{55}	942		966	47υ(C−N)$_{Me}$,26υ(C−C) 17δ(C−C)
ν_{24}	1484		1527	71τ(C−N)$_{Me}$,22δ(C−H)$_{Me}$	ν_{56}	921		941	43υ(C−C),32δ(C−C)
ν_{26}	1442	1445	1508	65υ(C−C),10δ(C−N)					10δ(N═N)
ν_{28}	1422	1427	1486	38υ(C−C),22υ(N−O) 17δ(C−N),10δ(C−C)	ν_{58}	860	867	881	98γ(C−H)
					ν_{60}	826	818	862	42δ(C−C),40υ(C−C)
ν_{30}	1390	1399	1423	33υ(N═N),19υ(C_{Ph}−N_{Me}) 14υ(C−C)	ν_{61}	772		839	95γ(C−H)
					ν_{63}	757	742	775	86τ(C−C)
ν_{32}	1364	1369	1400	69υ(C−C)	ν_{64}	733		758	87τ(C−C)
ν_{35}	1307	1316	1351	47δ(C−H),19δ(C−N) 15υ(C−C), 11υ(C−N)	ν_{66}	690		692	62τ(C−C),15γ(C−H) 11γ(C−N)$_{NO}$, 11γ(N−O)
ν_{36}	1234	1245	1313	35υ(C−N),26υ(C−C) 25δ(C−C)	ν_{67}	672		683	64δ(C−C),14δ(C−N)
					ν_{68}	652		669	82δ(C−C),10δ(C−N)
ν_{37}	1259		1283	53υ(C−N)$_{Me}$,26υ(C−C)	ν_{69}	637		658	93δ(C−C)
ν_{38}	1331	1340	1279	52υ(N−O),32υ(C−N)$_{NO}$	ν_{70}		598	572	57δ(C−C),16δ(C−N)
ν_{39}	1198	1197	1245	29υ(C−C),26υ(C−N) 23δ(C−C),10δ(C−H)	ν_{71}	544	542	564	45δ(C−N),41δ(C−C)
					ν_{72}	533		562	54τ(C−C),27γ(C−H)
ν_{40}	1177		1220	28δ(C−C),26υ(C−C) 25δ(C−H)$_{Me}$,11υ(C_{Ph}−N_{Me})	ν_{73}	517		523	27δ(C−N),24δ(C−C) 21δ(N−O),12υ(C−C)
ν_{42}	1133	1137	1184	30υ(C−N),28δ(C−C) 21υ(C−C)	ν_{74}	499		520	61τ(C−C),21γ(C−H)
					ν_{75}	459		479	30δ(C−N),18δ(C−N)$_{Me}$ 17υ(C−C),12δ(C−C)
ν_{47}	1101	1106	1137	38υ(C−C),34δ(C−C) 17υ(C−N)$_{NO}$	ν_{78}	415		438	91τ(C−C)
ν_{49}	1068		1048	69γ(C−H),29τ(C−C)					

[a] υ, stretch; in-plane bend; γ, out-of-plane bend; τ, torsion.

1000, 975, 960, 942, 921, 860, 826, 772, 757, 733, 690, 672, 652, 637, 544, 533, 517, 499, 459, and 415 cm^{-1}. In Figure 4b is shown the Raman spectrum of NDAB measured at 630 nm excitation. The Raman fundamentals of NDAB are observed at 1595, 1445, 1427, 1399, 1369, 1340, 1316, 1245, 1197, 1137, 1106, 1002, 955, 867, 818, 742, 598, and 542 cm^{-1}. It is observed from the figure that the most intense Raman bands appear at 1137, 1340, and 1399 cm^{-1}, followed by 1106, 1427, 1445, 1595, 1197, and 1002 cm^{-1}. A few weak bands are observed at 1369, 1316, 1245, 1002, 955, 867, 818, and 742 cm^{-1}. The calculated IR spectrum, also shown in Figure 4a is plotted by introducing a lorenzian broadening of 7 cm^{-1} similar to the case of NAB and DAB. An overview of the experimental and calculated IR intensity patterns show reasonable agreement. Thus, the IR bands are assigned by comparison of the calculated and experimental intensities as well as wavenumbers. The computed (unscaled) frequencies as well as the PEDs of various vibrational modes of NDAB along with the experimentally observed FTIR and Raman frequencies are listed in Table 6. The frequencies and PEDs of vibrations which are not observed experimentally are available as Supporting Information, Table S5. The calculated frequencies for the experimentally observed vibrations of the isotopomers of NDAB, viz. $NO_2C_6H_4N_1{}^{15}N_2C_6H_4N(CH_3)_2$, $NO_2C_6H_4N_1N_2{}^{15}C_6H_4N(CH_3)_2$, and $NO_2C_6H_4N_1{}^{15}N_2{}^{15}C_6H_4N(CH_3)_2$, are displayed in Table 7 along with the calculated IR intensities, while the results from all other vibrations are available as Supporting Information, Table S6. For NDAB, since no experimental data is available for the given isotopes, our discussion is mainly confined to the theoretically calculated isotopic shifts. As in the case of DAB, since the structure of NDAB is nonplanar, there is considerable mixing of the ip and oop vibrations.

In NDAB, the fundamental vibrations have contributions from the *N*,*N*-dimethylamino group (similar to DAB) as well as nitro group (as in the case of NAB). The vibrations υ_{15}, υ_{16}, υ_{17}, υ_{19}, υ_{26}, υ_{28}, υ_{39}, υ_{47}, and υ_{56} are assigned to the C−C stretch and are coupled to the C−C/C−H/ C−N ip bend. The fundamental mode, υ_{32} is assigned purely to the C−C stretch. Among these C−C stretching vibrations υ_{15}, υ_{26}, υ_{28}, υ_{32}, υ_{39}, and υ_{47} appear both in the FTIR (Raman) spectra at 1601 (1595), 1442 (1445), 1422 (1427), 1364 (1369), 1198 (1197), and 1101 (1106) cm^{-1} while the modes υ_{16}, υ_{17}, υ_{19}, and υ_{56} are observed only in the FTIR spectrum at 1590, 1557, 1515 and 921 cm^{-1} with intensities in agreement with the calculated spectrum. Two fundamentals belonging to this group, viz. υ_{39} and υ_{56}, as shown in Table 7, undergo subsequent shift in frequency of 1−2−3 and 8−8−17 cm^{-1} upon N^{15} isotopic substitution ($N_1{}^{15}$−$N_2{}^{15}$−$N_1{}^{15}N_2{}^{15}$). The mode υ_{24} is assigned to the methyl C−N torsion and is coupled to the methyl C−H ip bend. It is observed at 1485 cm^{-1} as a weak band in the FTIR spectrum and undergoes almost negligible change in frequency upon N^{15} isotopic substitution. It is observed from Table 6 that this mode has considerable mixing of the oop and ip vibrations. The mode υ_{38} corresponds to the N−O stretch and is coupled to the C−N(NO) stretch. It appears both in FTIR and Raman spectra at 1331 and 1340 cm^{-1}, respectively. Here, it is found that the experimentally observed frequency for the N−O stretch appears at higher wavenumbers as compared to that computed (1279 cm^{-1}) using B3LYP with 6-31G basis. The calculated and observed (FTIR−Raman) N−O stretching vibration for NDAB appears at 1279 and (1331−1340) cm^{-1}, respectively, which is at lower wavenumbers than that observed in the case of NAB where it appears at 1288 and (1343−1348) cm^{-1}. The lowering in frequency of the N−O stretch in NDAB as compared to NAB is in agreement with the trend observed for the calculated N−O bond length. The N−O stretching vibration, as expected, does not show any shift in frequency upon isotopic substitution of the azo N atoms. The vibration υ_{30} appearing at the calculated frequency of 1423 cm^{-1} corresponds to the N═N stretch and is coupled to the C(Ph)−N(Me) and C−C stretches. Experimentally, the fundamental corresponding to the N═N stretch is observed at 1390 (medium intensity) and 1399 cm^{-1} in the

TABLE 7: Calculated Frequencies for Isotopic Dervatives of 4-Nitro,4′-dimethylamino-azobenzene, Obtained from B3LYP/6-31G

		$C_{14}H_{14}N_1N_2NNO_2$				$C_{14}H_{14}N^{15}{}_1N_2NNO_2$		$C_{14}H_{14}N_1N^{15}{}_2NNO_2$		$C_{14}H_{14}N^{15}{}_1N^{15}{}_2NNO_2$	
mode	character	FTIR	Raman	calcd	I^a	calcd	I^a	calcd	I^a	calcd	I^a
ν_{15}	υ(C−C)	1601s	1595	1671	498.9	1671	493.2	1671	498.3	1670	492.1
ν_{16}	υ(C−C)	1590s		1653	263.8	1653	299.8	1653	291.1	1652	324.1
ν_{17}	υ(C−C)	1557m		1638	49.4	1638	55.8	1638	59.9	1638	65.8
ν_{19}	υ(C−C)	1515s		1581	193.9	1581	195.7	1581	187.5	1581	190.3
ν_{24}	τ(C−N)$_{Me}$	1484w		1527	0.0	1527	0.0	1527	0.0	1527	0.0
ν_{26}	υ(C−C)	1442w	1445	1508	6.2	1507	1.8	1507	2.5	1507	0.7
ν_{28}	υ(C−C)	1422m	1427	1486	63.7	1486	65.5	1486	68.7	1486	70.2
ν_{30}	υ(N═N)	1390m	1399	1423	23.6	1391	619.4	1394	676.9	1361	560.9
ν_{32}	υ(C−C)	1364s	1369	1400	347.5	1403	37.6	1403	47.4	1402	19.4
ν_{35}	δ(C−H)	1307m	1316	1351	23.6	1349	60.7	1351	21.9	1348	149.0
ν_{36}	υ(C−N)	1234w	1245	1313	3.1	1309	2.3	1309	0.6	1305	1.0
ν_{37}	υ(C−N)$_{Me}$	1259m		1283	29.7	1283	30.6	1283	29.3	1283	29.8
ν_{38}	υ(N−O)	1331s	1340	1279	1100.5	1279	1115.6	1279	1121.7	1279	1146.9
ν_{39}	υ(C−C)	1198m	1197	1245	96.5	1244	119.6	1243	126.7	1242	153.9
ν_{40}	δ(C−C)	1177w		1220	10.0	1220	6.5	1220	7.2	1220	4.3
ν_{42}	υ(C−N)	1133s	1137	1184	735.0	1182	776.4	1181	686.3	1179	715.1
ν_{47}	υ(C−C)	1101s	1106	1137	156.6	1137	165.6	1137	171.3	1137	181.3
ν_{49}	γ(C−H)	1068sh		1048	0.0	1048	0.0	1048	0.0	1048	0.0
ν_{51}	δ(C−C)	1000w	1002	1034	0.1	1034	0.1	1034	0.2	1034	0.2
ν_{53}	τ(C−C)	975sh		1029	0.5	1029	0.5	1029	0.5	1029	0.5
ν_{54}	τ(C−C)	960sh	955	1003	0.3	1003	0.3	1003	0.3	1003	0.3
ν_{55}	υ(C−N)$_{Me}$	942m		966	48.9	965	46.8	966	48.6	965	46.8
ν_{56}	υ(C−C)	921sh		941	0.7	933	0.7	933	0.8	924	0.9
ν_{58}	γ(C−H)	860m	867	881	2.3	881	2.3	881	2.3	881	2.3
ν_{60}	δ(C−C)	826m	818	862	35.4	859	33.7	860	41.1	857	39.1
ν_{61}	γ(C−H)	772w		839	1.2	839	1.2	839	1.2	839	1.2
ν_{63}	τ(C−C)	757w	742	775	0.6	775	0.6	775	0.6	774	0.6
ν_{64}	τ(C−C)	733w		758	3.9	758	3.8	758	3.9	758	3.8
ν_{66}	τ(C−C)	690m'		692	21.9	692	21.9	692	21.9	692	21.9
ν_{67}	δ(C−C)	672sh		683	0.3	682	0.2	680	0.6	680	0.4
ν_{68}	δ(C−C)	652sh		669	2.6	668	2.4	668	2.2	667	2.1
ν_{69}	δ(C−C)	637w		658	1.1	658	1.1	658	1.1	658	1.1
ν_{70}	δ(C−C)		598	572	2.6	571	3.2	571	3.4	570	3.8
ν_{71}	δ(C−N)	544m	542	564	15.6	561	12.7	561	12.7	559	12.6
ν_{72}	τ(C−C)	533m		562	12.6	561	14.2	561	13.8	561	12.7
ν_{73}	δ(C−N)	517w		523	7.1	523	7.3	522	7.5	522	7.7
ν_{74}	τ(C−C)	499sh		520	0.0	520	0.0	520	0.1	520	0.1
ν_{75}	δ(C−N)	459w		479	6.4	478	6.9	478	6.8	476	7.4
ν_{78}	τ(C−C)	415w		438	0.0	438	0.0	438	0.0	438	0.0

[a] *I* represents the infrared intensities in km/mol sh, shoulder; m, medium; s, strong, w, weak.

FTIR and Raman spectra, respectively. The azo stretching vibration shows a remarkable shift in frequency of 32, 29, and 62 cm^{-1} when either N_1, N_2 or both N_1 and N_2 is isotopically substituted by N^{15}. The fundamental mode υ_{35} is assigned to the C−H ip bend and is coupled to the C−N ip bend, C−C and C−N stretches, and is observed both in the FTIR and Raman spectra at 1307 (medium intensity) and 1316 cm^{-1}. It also shows a slight shift of 2−0−3 cm^{-1} upon N^{15} substitution ($N_1{}^{15}$−$N_2{}^{15}$−$N_1{}^{15}N_2{}^{15}$). The vibrations υ_{36} and υ_{42} are assigned to the C−N asymmetric and symmetric stretch, respectively, and are coupled to the C−C stretch and the C−C ip bend. The asymmetric and symmetric C−N stretching modes υ_{36} and υ_{42} are observed in the FTIR (Raman) spectra at 1234 (1245) and 1133 (1137) cm^{-1}. The asymmetric and symmetric C−N stretches are observed with weak and strong intensities, respectively, as predicted by our calculation. These asymmetric and symmetric C−N stretching vibrations undergo a change in frequency of 4−4−8 and 2−3−5 cm^{-1} upon N^{15} substitution ($N_1{}^{15}$−$N_2{}^{15}$−$N_1{}^{15}N_2{}^{15}$). The modes υ_{37} and υ_{55} correspond to the methyl C−N stretch and are coupled to the C−C stretch with additional coupling from the C−C ip bend in the case of the latter. The FTIR spectrum of NDAB as observed in Figure 4a display the appearance of the vibrations υ_{37} and υ_{55} at 1259 and 942 cm^{-1} with medium intensity. These fundamental modes donot show any shift in frequency upon isotopic substitution of the azo N atoms. The fundamentals υ_{40}, υ_{51}, υ_{60}, υ_{67}, υ_{68}, and υ_{70} are assigned to the C−C ip bend and have contributions from various vibrations, viz. C−C, C(Ph)−N(Me) stretches, methyl C−H, C−N ip bend, etc. The fundamental vibration υ_{69} is assigned purely to the C−C ip bend. The modes υ_{51} and υ_{60} are both FTIR (Raman) active and appear at 1000 (1002) and 826 (818) cm^{-1}, respectively. The vibration υ_{70} is Raman active and appears at 598 cm^{-1}, while the modes υ_{40} and υ_{67}−υ_{69} are FTIR active showing their appearances at 1177, 672, 652, and 637 cm^{-1}. Most of the C−C ip bending modes do not change in frequency upon N^{15} substitution ($N_1{}^{15}$−$N_2{}^{15}$−$N_1{}^{15}N_2{}^{15}$), except υ_{60} which suffers a reduction of 3−2−5 cm^{-1}. The mode υ_{49} is assigned to the C−H oop bend and is coupled to the C−C torsion, whereas the vibrations υ_{58} and υ_{61} are assigned purely to the C−H oop bends as observed from the calculated PEDs in Table 6. The pure oop C−H bending mode υ_{58} is both FTIR and Raman active and is observed at 860 and 867 cm^{-1} while υ_{49} and υ_{61} display only FTIR activity at 1068 and 772 cm^{-1}, respectively. These modes undergo no change upon N^{15} substitution. The vibrations υ_{53}, υ_{54}, υ_{66}, υ_{72}, and υ_{74} are assigned to the C−C torsion. All these fundamental modes are coupled to the C−H oop bend. Similarly, the fundamentals υ_{63}, υ_{64}, and υ_{78} are assigned purely to the C−C torsion. A few of these modes corresponding to the C−C torsion, viz. υ_{53}, υ_{64}, υ_{66}, υ_{72}, υ_{74}, and υ_{78}, appear in the FTIR spectrum of NDAB at 975,

733, 690, 533, 499, and 415 cm^{-1}, while the vibrations υ_{54} and υ_{63} are observed both in the FTIR (Raman) spectra at 960 (955) and 757 (742) cm^{-1}. The modes υ_{71}, υ_{73}, and υ_{75} are assigned to the C−N ip bends and are coupled to the C−C ip bends. The vibrational mode υ_{71} appears both in the FTIR and Raman spectra at 544 (medium intensity) and 542 cm^{-1}, while υ_{73} and υ_{75} are observed only in the FTIR spectrum at 517 and 459 cm^{-1}, respectively, with weak intensity. The modes υ_{71} and υ_{75} undergo a downshift in frequency of 3−3−5 and 1−1−3 cm^{-1} upon N^{15} substitution ($N_1{}^{15}-N_2{}^{15}-N_1{}^{15}N_2{}^{15}$). An overall comparison of the calculated and experimental (FTIR and Raman) frequencies in the case of NDAB show an excellent agreement. Except for a few vibrations, viz. υ_{17}, υ_{40}, υ_{58}, υ_{73}, and υ_{75}, where there are discrepancies, the calculated IR intensities are in reasonable agreement with those observed experimentally.

Complete analysis of the observed PEDs of various vibrations in NAB, DAB and NDAB and a comparison of the experimental and calculated frequencies as well as the IR intensities, reveal the fact that B3LYP with 6-31G basis set provides a very good agreement with the experimentally observed FTIR and Raman frequencies as well as the IR intensities. This computational method although slightly overestimates the calculated frequencies relative to the experimental values for most vibrations, except for the N−O stretch as observed in the case of NAB and NDAB, where it is found to underestimate the experimental frequency, but provides a reasonable one to one correspondence to the experimental frequencies. It is also observed that the IR intensities are essential for the assignment of the vibrational spectra.

Summary

Overall, the essential differences between the vibrational spectra of NAB, DAB, and NDAB can be summarized as follows: NAB is planar, whereas DAB and NDAB are completely nonplanar. Due to the nonplanarity in the structure of DAB and NDAB, there is considerable mixing of the ip and oop modes. Moreover, the π-electron density on the central N═N bond is maximum in NAB and it decreases in DAB as well as NDAB due to the increased π-conjugation. This increase in the π-conjugation in DAB and NDAB leads to a decrease in double bond character for N═N. As a result the main azo stretching vibration of NAB, υ(N═N) appears at higher frequency (1462 cm^{-1}) as compared to DAB (1442 cm^{-1}) and NDAB (1423 cm^{-1}). In addition, a reverse trend is observed for the C−N stretching vibration. NAB exhibits more single bond character for the C−N bond, because of which υ(C−N) appears at lower wavenumber (1272 cm^{-1}) relative to DAB (1300 cm^{-1}) and NDAB (1313 cm^{-1}).

A systematic study of the vibrational analysis of NAB, DAB, and NDAB using FTIR, Raman and hybrid HF/DFT method, B3LYP with the 6-31G basis set is carried out. It is observed that the hybrid DFT method is very useful in predicting accurate vibrational structure and frequencies for polyatomic systems such as NAB, DAB, and NDAB. Although the computed frequencies in general are slightly overestimated relative to the experimental FTIR and Raman frequencies, it provides a one-to-one correspondence between the computed and experimental frequencies. These computed frequencies and intensities are in good agreement with the experimental frequencies and IR intensities for all the acceptor, donor, and donor−acceptor substituted azobenzenes. Thus, we find that the performance of DFT approach for polyatomic molecules is of high quality for all the normal vibrations, facilitating accurate vibrational assignments of experimental data. We also point out the main differences in the vibrational spectra of NAB, DAB, and NDAB on the basis of their respective molecular structures.

Acknowledgment. We thank the Council of Scientific and Industrial Research and the Department of Science and Technology, Government of India for financial support, and the Supercomputer Education and Research Centre, Indian Institute of Science, for providing us the computing facilities necessary to carry out the present calculation.

Supporting Information Available: Tables of the calculated frequencies as well as the PEDs of NAB, DAB, and NDAB, and their isotopic analogues. Supporting Information is available free of charge via the Internet at http://pubs.acs.org.

References and Notes

(1) Rau, H. *Photochromism. Molecules and Systems*; Durr, H., Bouas-Laurent, H., Eds.; Elsevier: Amsterdam, 1990; Chapter 4, p 165.
(2) Zollinger, H. *Color Chemistry, Syntheses, Properties and Applications of Organic Dyes and Pigments*; VCH: New York, 1987; p 92.
(3) (a) Bach, H.; Anderle, K.; Fuhrmann, Th.; Wendorff, J. H. *J. Phys. Chem.* **1996**, *100*, 4135. (b) Liu, Z.; Zhao, C.; Tang, M.; Cai, S. *J. Phys. Chem.* **1996**, *100*, 17337. (c) Taniike, K.; Matsumoto, T.; Sato, T.; Ozaki, Y.; Nakashima, K.; Iriyama, K. *J. Phys. Chem.* **1996**, *100*, 15508.
(4) Ramanujam, P. S.; Hvilsted, S.; Andruzzi, F. *Appl. Phys. Lett.* **1993**, *62*, 1041.
(5) Lee, G. J.; Kim, D.; Lee, M. *Appl. Opt.* **1995**, *34*, 138.
(6) Ramanujam, P. S.; Hvilsted, S.; Zebger, I.; Siesler, H. W. *Macromol. Rapid. Commun.* **1995**, *16*, 455.
(7) Hvilsted, S.; Andruzzi, F.; Ramanujam, P. S. *Opt. Lett.* **1992**, *17*, 1234.
(8) Willner, I.; Rubin, S. *Angew. Chem., Int. Ed. Engl.* **1996**, *35*, 367.
(9) Cimiraglia, R.; Hofmann, H.-J. *Chem. Phys. Lett.* **1994**, *217*, 430.
(10) Rau, H.; Yu-Quan, S. *J. Photochem. Photobiol. A* **1988**, *42*, 321.
(11) Cimiraglia, R.; Asano, T.; Hofmann, H.-J. *Gazz. Chim. Ital.* **1996**, *126*, 679.
(12) Hamm, P.; Ohline, S. M.; Zinth, W. *J. Chem. Phys.* **1997**, *106*, 519.
(13) Asano, T.; Cosstick, K.; Furuta, H.; Matsuo, K.; Sumi, H. *Bull. Chem. Soc. Jpn.* **1996**, *69*, 551.
(14) Sanchez, A. M.; de Rossi, R. H. *J. Org. Chem.* **1996**, *61*, 3446.
(15) Biswas, N.; Umapathy, S. *Chem. Phys. Lett.* **1995**, *234*, 24.
(16) Biswas, N.; Umapathy, S. *J. Chem. Phys.*, **1997**, *107*, 7849.
(17) Biswas, N.; Umapathy, S. *J. Phys. Chem. A* **1997**, *101*, 5555.
(18) Lednev, I. K.; Ye, T.-Q.; Hester, R. E.; Moore, J. N. *J. Phys. Chem.* **1996**, *100*, 13338.
(19) Monti, S.; Orlandi, G.; Palmieri, P. *Chem. Phys.* **1982**, *71*, 87.
(20) Rau, H.; Luddecke, E. *J. Am. Chem. Soc.* **1982**, *104*, 1616.
(21) Rau, H. *J. Photochem.* **1984**, *26*, 221.
(22) Sampiringue, N.; Guyot, G.; Monti, S.; Bortolus, P. *J. Photochem.* **1987**, *37*, 185.
(23) Lunak, S., Jr.; Nepras, M.; Hrdina, R.; Mustroph, H. *Chem. Phys.* **1994**, *184*, 255.
(24) Dyck, R. H.; McClure, D. S. *J. Chem. Phys.* **1962**, *36*, 2326.
(25) Kübler, V. R.; Lüttke, W.; Weckherlin, S. *Z. Elektrochem.* **1960**, *64*, 650.
(26) Okamoto, H.; Hamaguchi, H.; Tasumi, M. *Chem. Phys. Lett.* **1986**, *130*, 185.
(27) Biancalana, A.; Campani, E.; Gorini, G.; Masetti, G.; Quaglia, M. *J. Raman. Spectrosc.* **1992**, *23*, 155.
(28) Biancalana, A.; Campani, E.; Domenico, G. Di; Gorini, G.; Masetti, G.; Quaglia, M. *J. Raman. Spectrosc.* **1993**, *24*, 43.
(29) Lorriaux, J. L.; Merlin, J. C.; Dupaix, A.; Thomas, E. W. *J. Raman Spectrosc.* **1979**, *8*, 81.
(30) Machida, K.; Lee, H.; Saito, Y.; Uno, T. *J. Raman Spectrosc.* **1978**, *7*, 184.
(31) Hacker, H. *Spectrochim. Acta* **1965**, *21*, 1989.
(32) Merlin, J. C.; Lorriaux, J. L.; Thomas, E. W.; Dupiax, A. *J. Raman Spectrosc.* **1981**, *11*, 209.
(33) Cataliotti, R. S.; Murgia, S. M.; Paliani, G.; Poletti, A.; Zgierski, M. Z. *J. Raman. Spectrosc.* **1985**, *16*, 251.
(34) Cataliotti, R. S.; Murgia, S. M.; Paliani, G.; Poletti, A.; Zgierski, M. Z. *J. Raman. Spectrosc.* **1985**, *16*, 258.
(35) Cataliotti, R. S.; Morresi, A.; Paliani, G.; Poletti, A.; Zgierski, M. Z. *J. Raman. Spectrosc.* **1989**, *20*, 601.
(36) Barker, I. K.; Fawcett, V.; Long, D. A. *J. Raman Spectrosc.* **1987**, *18*, 71.

(37) Houben, J. L.; Masetti, G.; Campani, E.; Gorini, G. *J. Raman Spectrosc.* **1982**, *13*, 15.
(38) Armstrong, D. R.; Clarkson, J.; Smith, W. E. *J. Phys. Chem.* **1995**, *99*, 17825.
(39) Bell, S.; Bisset, A.; Dines, T. J. *J. Raman Spectrosc.* **1998**, *29*, 447.
(40) Negri, F.; Orlandi, G. *J. Raman Spectrosc.* **1998**, *29*, 501.
(41) Stepanian, S. G.; Reva, I. D.; Radchenko, E. D.; Adamowicz, L. *J. Phys. Chem. A* **1999**, *103*, 4404.
(42) Wheeler, D. E.; Rodriguez, J. H.; McCusker, J. K. *J. Phys. Chem. A* **1999**, *103*, 4101.
(43) Pan, D.; Phillips, D. L. *J. Phys. Chem. A* **1999**, *103*, 4737.
(44) Stephens, P. J.; Devlin, F. J.; Chablowski, C. F.; Frisch, M. J. *J. Phys. Chem.* **1994**, *98*, 11623.
(45) (a) Handy, N. C.; Maslen, P. E.; Amos, R. D.; Andrews, J. S.; Murray, C. W.; Laming, G. J. *Chem. Phys. Lett*. **1992**, *197*, 506. (b) Handy, N. C.; Murray, C. W.; Amos, R. D. *J. Phys. Chem.* **1993**, *97*, 4392.
(46) (a) El-Azhary, A. A.; Suter, H. U. *J. Phys. Chem.* **1995**, *99*, 12751. (b) El-Azhary, A. A.; Suter, H. U. *J. Phys. Chem.* **1996**, *100*, 15056.
(47) Boesch, S. E.; Wheeler, R. A. *J. Phys. Chem.* **1995**, *99*, 8125.
(48) Walden, S. E.; Wheeler, R. A. *J. Phys. Chem.* **1996**, *100*, 1530.
(49) Wong, M. W. *Chem. Phys. Lett.* **1996**, *256*, 391.
(50) (a) Lee, S. Y.; Boo, B. H. *J. Phys. Chem.* **1996**, *100*, 8782. (b) Lee, S. Y.; Boo, B. H. *J. Phys. Chem.* **1996**, *100*, 15073.
(51) (a) Nonella, M.; Brandli, C. *J. Phys. Chem.* **1996**, *100*, 14549. (b) Nonella, M.; Tavan, P. *Chem. Phys.* **1995**, *199*, 17.
(52) Wheeless, C. J. M.; Zhou, X.; Liu, R. *J. Phys. Chem.* **1995**, *99*, 12488.
(53) (a) Keszthelyi, T.; Wilbrandt, R.; Bally, T.; Roulin, J.-L. *J. Phys. Chem.* **1996**, *100*, 16850. (b) Keszthelyi, T.; Wilbrandt, R.; Bally, T. *J. Phys. Chem.* **1996**, *100*, 16843.
(54) Walden, S. E.; Wheeler, R. A. *J. Phys. Chem.* **1996**, *100*, 1530.
(55) Kwiatkowski, J. S.; Leszczynski, J. *J. Phys. Chem.* **1996**, *100*, 941.
(56) Qin, Y.; Wheeler, R. A. *J. Phys. Chem.* **1996**, *100*, 10554.
(57) Mohandas, P.; Umapathy, S. *J. Phys. Chem. A* **1997**, *101*, 4449.
(58) Hout, Jr. R. F.; Levi, B. A.; Hehre, W. J. *J. Comput. Chem.* **1982**, *3*, 234.
(59) Heller, E. J. *Acc. Chem. Res.* **1981**, *14*, 368. (b) Myers, A. B.; Mathies, R. A. *Biological Applications of Raman Spectroscopy*; Spiro, T. G., Ed.; Wiley: New York, 1987; Vol. 2, p 1. (c) Myers, A. B. *Laser Techniques in Chemistry*; Myers, A. B., Rizzo, T. R., Eds.; Wiley: New York, 1995; Vol. 23, p 325.
(60) Frisch, M. J.; Trucks, G. W.; Schlegel, H. B.; Gill, P. M. W.; Johnson, B. G.; Robb, M. A.; Cheeseman, J. R.; Keith, T.; Petersson, G. A.; Montgomery, J. A.; Raghavachari, K.; Al-Laham, M. A.; Zakrzewski, V. G.; Ortiz, J. V.; Foresman, J. B.; Cioslowsski, J.; Stefanov, B. B.; Nanayakkara, A.; Challacombe, M.; Peng, C. Y.; Ayala, P. Y.; Chen, W.; Wong, M. W.; Andres, J. L.; Replogle, E. S.; Gomperts, R.; Martin, R. L.; Fox, D. J.; Binkley, J. S.; Defrees, D. J.; Baker, J.; Stewart, J. P.; Head-Gordon, M.; Gonzalez, C.; Pople, J. A. *Gaussian 94*, Revision C.2; Gaussian, Inc., Pittsburgh, PA, 1995.
(61) Becke, A. D. *J. Chem. Phys.* **1993**, *98*, 5648.
(62) Becke, A. D. *Phys. Rev. A* **1988**, *38*, 3098.
(63) Lee, C.; Yang, W.; Parr, R. G. *Phys. Rev. B* **1988**, *37*, 785.
(64) Schlegel, H. B. *J. Comput. Chem.* **1982**, *3*, 214.
(65) Ulman, A.; Willand, C. S.; Köhler, W.; Robello, D. R.; Williams, D. J.; Handley, L. *J. Am. Chem. Soc.* **1990**, *112*, 7083.
(66) Traetteberg, M.; Hilmo, I.; Hagen, K. *J. Mol. Struct.* **1977**, *39*, 231.